frontiers in Earth Science

ORIGINAL RESEARCH
published: 24 November 2021
doi: 10.3389/feart.2021.757749

High-Resolution Late Devonian Magnetostratigraphy From the Canning Basin, Western Australia: A Re-Evaluation

Theodore Green[1†], *Sarah P. Slotznick*[1*], *Plinio Jaqueto*[2], *Timothy D. Raub*[3], *Eric Tohver*[2], *Ted E. Playton*[4], *Peter W. Haines*[5], *Joseph L. Kirschvink*[6,7], *Roger M. Hocking*[5‡] and *Paul Montgomery*[4‡]

[1]Department of Earth Sciences, Dartmouth College, Hanover, NH, United States, [2]Instituto de Astronomia, Geofísica e Ciências Atmosféricas, Universidade de São Paulo, São Paulo, Brazil, [3]School of Earth and Environmental Sciences, University of St. Andrews, St. Andrews, United Kingdom, [4]Frontier Exploration and Appraisal, Chevron, Houston, TX, United States, [5]Geological Survey of Western Australia, East Perth, WA, Australia, [6]Division of Geological and Planetary Sciences, California Institute of Technology, Pasadena, CA, United States, [7]Earth-Life Science Institute, Tokyo Institute of Technology, Tokyo, Japan

Late Devonian time was a period of rapid upheaval in the Earth system, including climate change, sea level changes, widespread ocean anoxia, and the Frasnian-Famennian mass extinction; the cause(s) of these changes remain(s) uncertain. The Lennard Shelf of the Canning Basin in Western Australia contains carbonate reef sections spanning much of the Late Devonian Epoch and has been sampled for paleomagnetic analysis with studies by Hansma and colleagues in 2015 and Playton and colleagues in 2016. However, previous paleomagnetic directions were scattered and their use for magnetostratigraphy has been questioned. Here, rock magnetic data and magnetostratigraphy for a late Devonian drill-core from the Lennard Shelf were analyzed. Three magnetostratigraphic interpretations were made using different paleopoles that showed good correlation with each other and the earlier interpretations by Playton and colleagues in 2016. Additionally, the rock magnetic data revealed the samples contain various mixtures of detrital and diagenetic minerals, the former of which should be viable recorders of primary magnetic signatures. Even in samples with these detrital phases, paleomagnetic data were often noisy and produced ambiguous polarity assignments, likely due to the anomalously weak Devonian field. Because of this ambiguity and the absence of a robust paleopole, broader correlations for this critical time-period will be difficult without additional paleomagnetic data from the late Devonian Period. Expanded data for this interval could eventually shed light on the timing, causes, and rates of the Frasnian-Famennian mass extinction and other environmental shifts in the late Devonian Epoch.

Keywords: Devonian, Canning Basin, Frasnian-Famennian mass extinction, magnetostratigraphy, rock magnetism, Earth's magnetic field

OPEN ACCESS

Edited by:
Eric Font,
University of Coimbra, Portugal

Reviewed by:
Stefanie Brachfeld,
Montclair State University, United States
Rui Zhang,
Northwest University, China

****Correspondence:***
Sarah P. Slotznick
sslotz@dartmouth.edu

†Present address:
Theodore Green,
Department of Geosciences, Princeton University, Princeton, NJ, United States

‡Retired

Specialty section:
This article was submitted to Geomagnetism and Paleomagnetism, a section of the journal Frontiers in Earth Science

Received: *12 August 2021*
Accepted: *27 September 2021*
Published: *24 November 2021*

Citation:
Green T, Slotznick SP, Jaqueto P, Raub TD, Tohver E, Playton TE, Haines PW, Kirschvink JL, Hocking RM and Montgomery P (2021) High-Resolution Late Devonian Magnetostratigraphy From the Canning Basin, Western Australia: A Re-Evaluation. Front. Earth Sci. 9:757749. doi: 10.3389/feart.2021.757749

1 INTRODUCTION

The Devonian Period had expansive reefs that contributed to abundant carbonate production and the greatest marine diversity of the Paleozoic Era, including the appearance and diversification of aquatic tetrapods (e.g., Becker et al., 2020; Bambach et al., 2002; Kiessling et al., 2003). The Late Devonian time-period in particular saw significant changes in global climate, sea level, and marine geochemical records (Hillbun et al., 2015, 2016). Despite overall high Devonian marine diversity, a protracted mass extinction event occurred during the Frasnian and Famennian stages that greatly decreased the abundance of marine and terrestrial life before and continuing into the Carboniferous Period (Percival et al., 2018). The Frasnian-Famennian mass extinction was especially destructive to the widespread Devonian reef systems and stromatoporoids (Percival et al., 2018) but, in the aftermath, lead to diversification of organisms like tetrapods, actinopterygians, and chondrichthyans that had previously comprised a less significant part of the biotic system (Sallan and Coates, 2010). Despite its place in the list of the five largest mass extinctions (Sepkoski, 2002) and importance for later vertebrate radiation, the causes of the Frasnian-Famennian extinction remain uncertain. The eruption of the Viluy or Kola-Dnieper Large Igneous Provinces, marine anoxia, orbital forcings, and extraterrestrial impact events have all been suggested as causes of the extinction (Ernst and Youbi, 2017; Percival et al., 2018; Lu et al., 2021), but poorly constrained Devonian chronostratigraphy and imprecise dating of the causal mechanisms have led to continued debate (e.g., Ricci et al., 2013; Ma et al., 2016; Percival et al., 2018; Lu et al., 2021).

The tool of choice for integrating paleontological observations and sedimentary stratigraphic successions is magnetostratigraphy, which uses primary magnetic field signals recorded in magnetic minerals to determine a characteristic pattern of polarity reversals that can then aid in correlating and dating sections (Butler, 1992; Langereis et al., 2010). However, the Earth's magnetic field is complex and difficult to constrain throughout the Devonian Period, which makes it challenging to compile accurate chronologies, including around the Frasnian-Famennian extinction (Hansma et al., 2015; Percival et al., 2018; Becker et al., 2020; van der Boon et al., 2021, in review; Ogg, 2020). Paleointensity is lower in the Devonian Period (Hawkins et al., 2019; Perrin and Shcherbakov, 1997; Shcherbakova et al., 2017); paleomagnetic samples often have complex overprinting and remagnetizations (Torsvik et al., 2012); reversals are more common than in other intervals (Hansma et al., 2015; Hounslow et al., 2018); and there are few robust paleopoles during this time (Torsvik et al., 2012; van der Boon et al., 2021, in review). The poles that do exist are often derived from older magnetic data that is not available at the measurement level for reassessment (van der Boon et al., 2021, in review; Torsvik et al., 2012). Globally there is a dearth of paleomagnetic data in the Devonian Period. The complex and frequently weak Devonian magnetic data could be attributed to a low-intensity, non-dipolar field (Shcherbakova et al., 2017; Hawkins et al., 2021) and/or a hyperreversal period of the magnetic field (Shcherbakova et al., 2019).

Regardless of causal reasons for the dearth of poles and ambiguous magnetic records, these consistent challenges with interpreting data in the Devonian Period lower the confidence in other stratigraphic and chronologic records correlated with them. More paleomagnetic data is essential for identifying potential causes of the complex Devonian magnetic signals, evaluating which data might be usable, and producing a Devonian Global Polarity Timescale (van der Boon et al., 2021, in review). Here we present a high-resolution magnetostratigraphic record and rock magnetic data for a late Devonian core from the Canning Basin, Australia and then compare the results to other poles and magnetostratigraphic records for the region.

2 GEOLOGIC SETTING

The Canning Basin in Western Australia (**Figure 1**) formed in the Ordovician Period and persisted through the Devonian Period as Gondwana underwent crustal extension, rifting, and subsidence around 10–15° south of the equator (Tyler et al., 2012; Hillbun et al., 2016; Playton et al., 2016). A carbonate reef system developed in the northeastern part of this sub-equatorial basin, creating the numerous carbonate outcrops of the Lennard Shelf over a 25-million-year interval in the Middle and Late Devonian Epochs (Playford et al., 2009; Playton et al., 2016). This transgressive-regressive carbonate supersequence consists of platform top, reef, slope, and basinal mixed carbonate-siliciclastic environments and is bordered by the Proterozoic North Australian Craton to the north and the Fitzroy Trough to the south, a fault-bounded sub-basin within the Canning Basin. The reefal depositional system today is well exposed with minimal structural deformation or overprinting.

In the Bugle Gap area of the Lennard Shelf exposures, the Canning Basin Chronostratigraphy Project (CBCP) collected drill cores using the shallow, portable, tripod-mounted Winkie drilling equipment at McWhae Ridge (MR1) and Wade Knoll (WK1) (Playton et al., 2016). Both cores are dominated by silty limestone representing distal slope and basinal settings. McWhae Ridge is a drowned reef spine, and the MR1 core penetrates younger, onlapping distal slope sediments ranging from Lower Frasnian to Lower Famennian in age according to moderately-constrained biostratigraphy data. The facies are mud-dominated, consisting of silty mudstones and wackestones with minor packstones. A distinctive iron-rich microbialite marker bed (locally identified as Frutexites, Playford et al., 2009) was observed at the drilling location of MR1 (base of bed is 0 m core depth) that constrains this uppermost stratigraphy to the Lowermost Famennian. The beds have shallow dips, between 10 and 15°, that are likely steepened by compaction around the McWhae Ridge reef spine. Wade Knoll is in Paddy's Valley between the Emmanuel and Laidlaw Ranges, and the WK1 core represents distal slope and basinal environments between the surrounding transgressive reefal margins. The depositional timing of WK1 is poorly constrained with few, imprecise biostratigraphic controls.

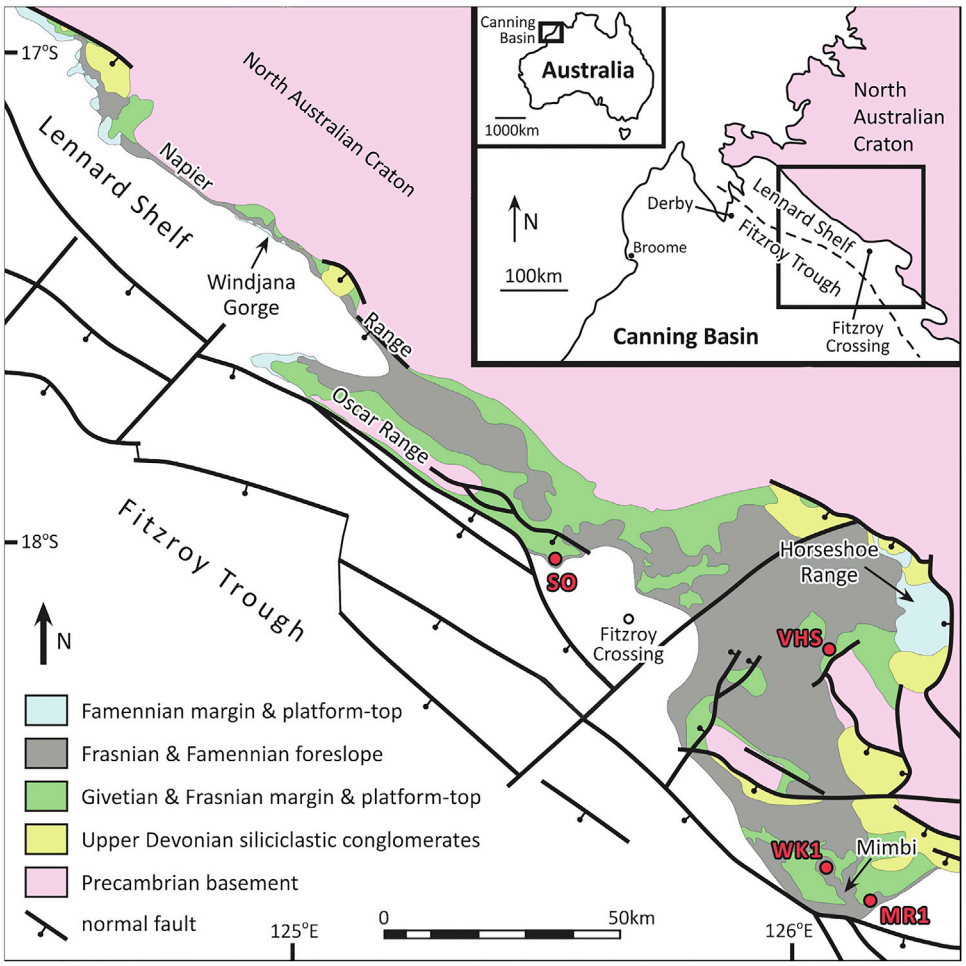

FIGURE 1 | Simplified geologic map of Lennard Shelf, Canning Basin. Simplified outcrop exposure and location maps for the Lennard Shelf, Canning Basin, Western Australia. Red labels indicate sites where paleomagnetic data was collected. SO = South Oscars measured section; VHS = Horse Spring measured section; WK1 = Wade Knoll Winkie core; MR1 = McWhae Ridge Winkie core. SO and VHS paleomagnetic data were analyzed and published in Hansma et al. (2015). Modified after Playton et al. (2016).

It does contain a Lower Frasnian marker bed, so it is interpreted to span part of the Lower Frasnian. It is similar to the mud-dominated MR1 facies, consisting of silty mudstone-wackestone-packstone with dips of 3° or less (Playton et al., 2016).

3 METHODS

The CBCP compiled samples from key outcrop transects, shallow Winkie cores, and subsurface cores to explore chronostratigraphic signals contained within different Middle-Late Devonian carbonate environments along the Lennard Shelf (Playton et al., 2016). The MR1 Winkie core is the focus of this study and is a 42.2 m long AW34 core drilled in July 2010 at 18° 43′ 59.61″S, 126° 4′ 46.02″E. The Winkie core was oriented using bedding planes (drilled at a 14° angle to them) and marking the top of each core run using a string (**Supplementary Figure S1**). A total of 155 samples (25-mm-diameter) were collected perpendicular to the core using a drill-press at the Geological Survey of Western Australia. The WK1 Winkie core is a 37.95 m long AW34 core also drilled in July 2010 at 18° 39′ 25.04″S, 126° 0′ 5.19″E with a total of 74 samples (25-mm-diameter) collected. The samples from both cores were further cut into specimens at the California Institute of Technology for paleomagnetic analyses, isotopic analyses, rock magnetic analyses, and archiving.

Rock magnetic data was conducted on 21 samples across the MR1 core using a 2G Enterprises SQuID magnetometer at the California Institute of Technology following the RAPID protocols (Kirschvink et al., 2008). This protocol included measuring alternating field demagnetization of the natural remanent magnetization (NRM); acquisition and demagnetization of anhysteretic remanent magnetization and isothermal remanent magnetization (IRM); and backfield IRM acquisition. The samples were analyzed using the MAX UnMix web application (Maxbauer et al., 2016). Together, these rock magnetic methods can be used to distinguish different ferromagnetic minerals on the

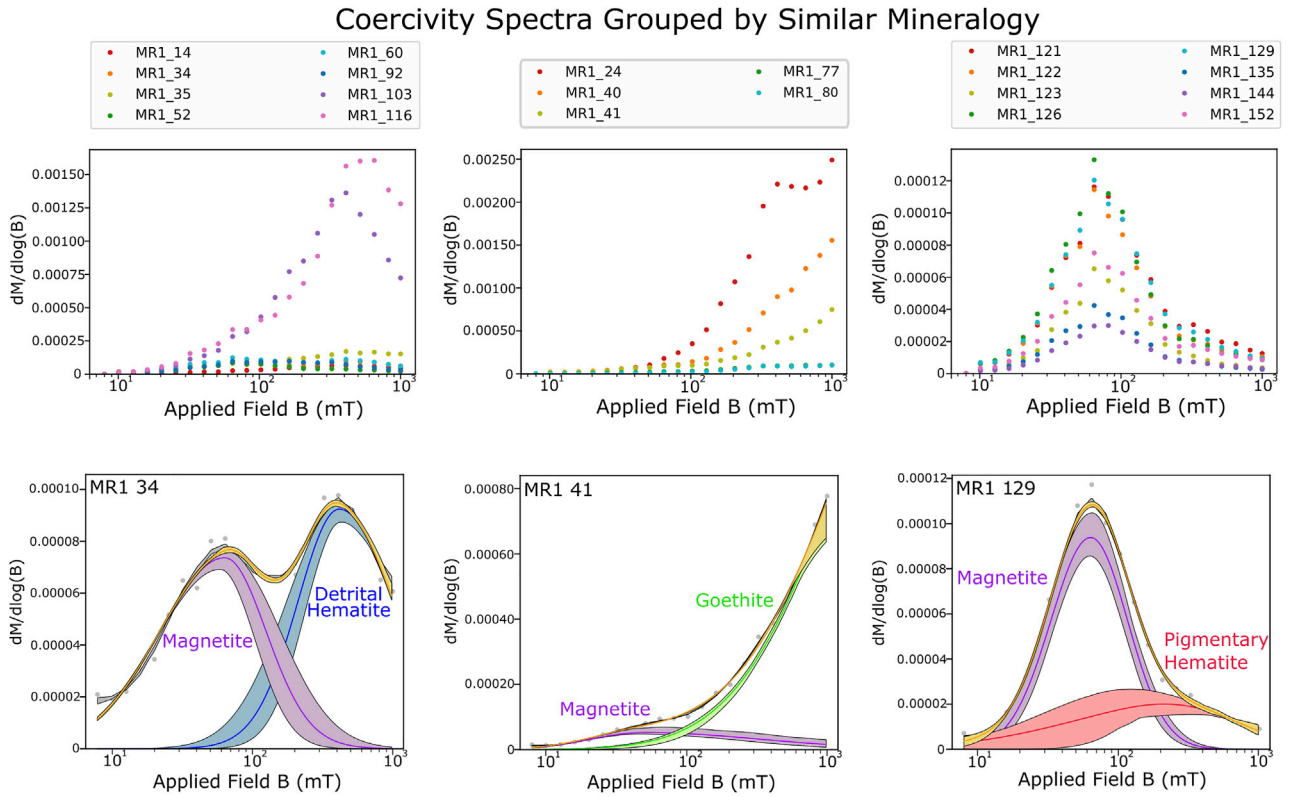

FIGURE 2 | Coercivity spectra and unmixed magnetic components for selected MR1 samples. Rock magnetic data were collected for 21 samples from the MR1 core (for stratigraphic location, see **Figure 4**). The unscaled coercivity spectra for those samples are shown here, separated by mineralogy, with detrital hematite-bearing samples on the **left,** goethite-bearing samples in the **center**, and pigmentary hematite-bearing samples on the **right**. The three samples that contain both detrital hematite and goethite are included in the goethite column. Below each coercivity spectra is a representative plot of the magnetic mineral components contained in those samples, made using MAX UnMix (Maxbauer et al., 2016). Eleven samples contain detrital hematite, five have goethite, eight have pigmentary hematite, and 20 have magnetite. Each sample contains some combination of two or three of these magnetic minerals, as shown in the MAX UnMix representative plots. Some of the peaks labelled as magnetite could instead be attributed to pyrrhotite based on the demagnetization data.

basis of observed fundamental properties (e.g., Peters and Dekkers, 2003). Previously unpublished rock magnetic analyses from five specimens from the VHS outcrops (Hansma et al., 2015) were also measured with the same procedure (**Supplementary Figure S2**).

The demagnetization routine, carried out at the California Institute of Technology using a 2G Enterprises SQuID magnetometer with an automated sample-changing system (Kirschvink et al., 2008), was similar for MR1 and WK1. It started by cooling the samples in liquid N_2 in a low-field space to remove viscous magnetizations. Two low-temperature cycling steps (−196°C) were followed by three low-intensity alternating field steps (2.3, 4.6, and 6.9 mT) to remove secondary magnetizations. The main demagnetization process was thermal. For MR1, steps at 60°C and 80°C were carried out in air before adding in a trickle of N_2 gas to minimize oxidation in subsequent steps. Steps of 5–30°C were used as the samples were heated from 100°C to 675°C. For WK1, a step at 75°C was carried out in air while all subsequent ones proceeded in N_2 gas. Steps of 5–25°C were used as samples were heated from 100°C to 320°C. Magnetic directions were determined for each sample using principle component analysis (Kirschvink, 1980) and the PmagPy software (Tauxe et al., 2016).

4 RESULTS

Following these rock magnetic protocols, the derivative of the IRM demagnetization was used to determine the coercivity of remanence and then fit using the MAX UnMix web application (Maxbauer et al., 2016) to identify the ferromagnetic minerals present in each sample (**Figure 2**; Peters and Dekkers, 2003). Using a smoothing factor of 0.4, four different components were identified, with two or three of those components appearing in any given sample. The highest coercivity component had a range of 1,100–1,950 mT. It was interpreted to be goethite and found in five of the samples. The 401–604 mT component was identified in 11 samples and attributed to hematite. The 110–407 mT component, found in eight samples, was labelled as finer-grained (a.k.a. "pigmentary") hematite (Swanson-Hysell et al., 2019). Present in 20 samples, the 27–116 mT component was interpreted as magnetite. Based on the thermal demagnetization patterns, pyrrhotite may be present instead of or in addition to

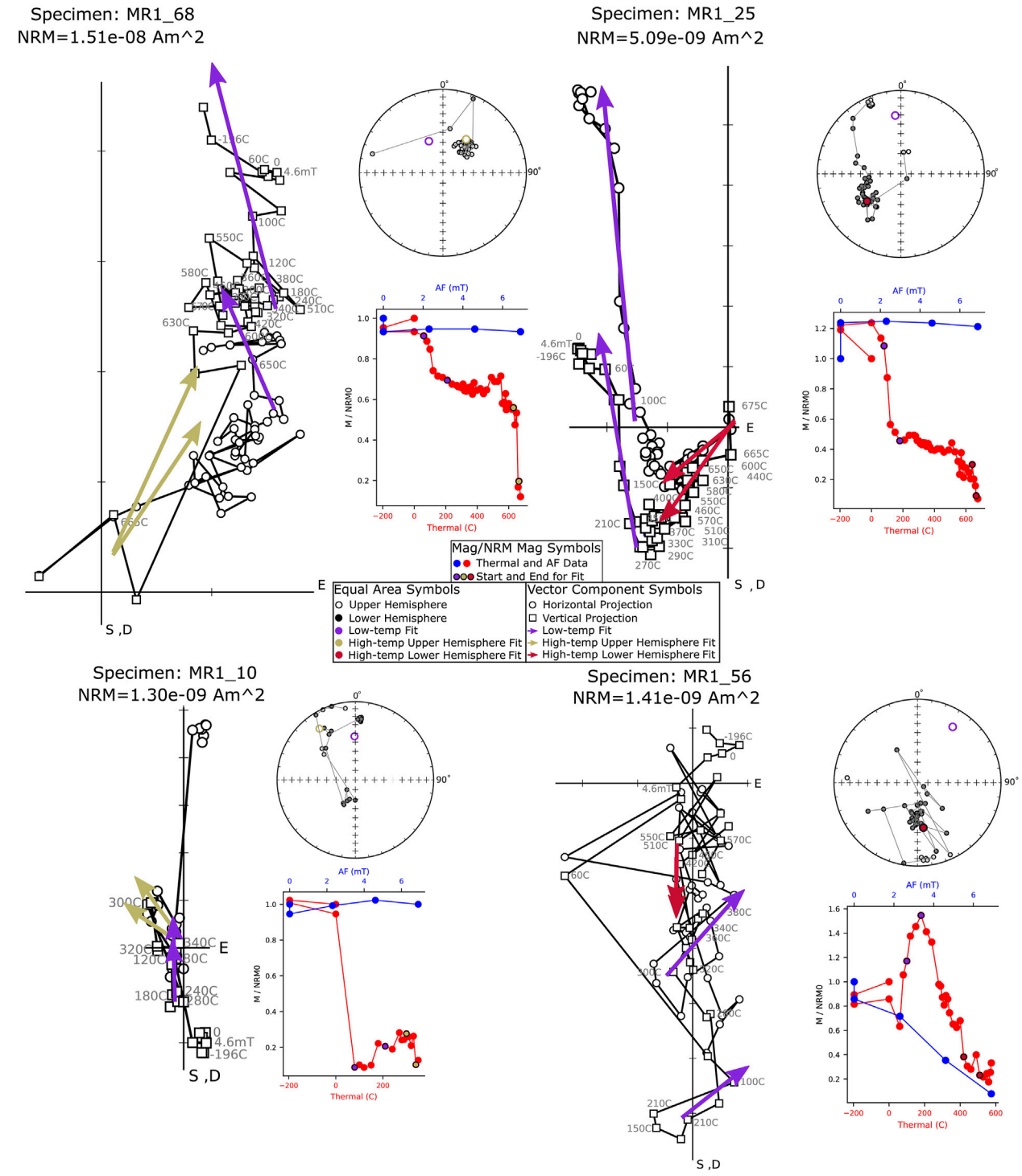

FIGURE 3 | Paleomagnetic data. Equal area, magnetization normalized to initial magnetization (M/NRM0, NRM = natural remanent magnetization), and Zijderveld plots of demagnetization data for four representative samples in the upper (samples MR1-68 and MR1-10) and lower (samples MR1-25 and MR1-56) hemispheres in tilt-corrected coordinates. MR1-68 and MR1-25 are among the best samples with well-defined, origin-reaching, high-temperature components and the high-blocking temperatures indicative of detrital hematite. MR1-10 and MR1-56 are noisier samples.

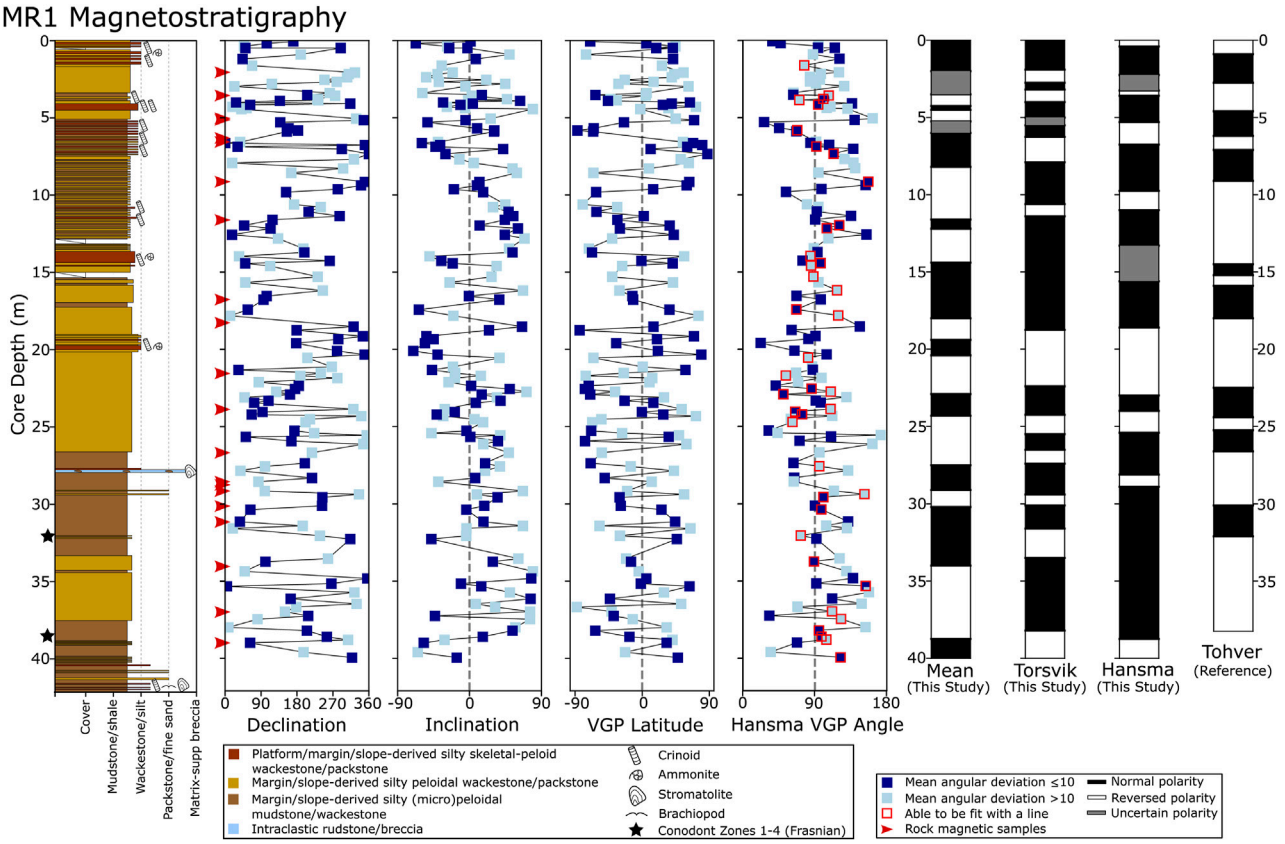

FIGURE 4 | Paleomagnetic directional data and magnetostratigraphy for MR1. Lithologic log, declination, inclination, and virtual geomagnetic pole (VGP) latitude data for the high-temperature components of MR1. The lithologic log is modified from Playton et al. (2016) and shows fossils and biostratigraphic markers in the section. Red arrows indicate the 21 locations where samples were taken for rock magnetic analysis. In the fifth column, the VGPs are plotted as an angle from the paleopole calculated by Hansma et al. (2015) for the Canning Basin; samples that could be fit with a line going to the origin instead of an anchored line are outlined in red. The same calculations and plotting were done using the angle from the mean VGP of the dataset and from the pole calculated by Torsvik et al. (2012) for Gondwana at 370 Ma (**Supplementary Figure S3**). The magnetic reversals determined from each of these different datasets were used to create a corresponding magnetostratigraphic record. For the magnetostratigraphic record that used the Hansma et al. (2015) paleopole, the meterage of the polarity changes is listed in **Supplementary Table S1**. The magnetostratigraphy for MR1 published in Playton et al. (2016) is labelled as Tohver data and compared to the magnetostratigraphy produced here. The Hansma et al. (2015), Torsvik et al. (2012), Playton et al. (2016) records are all fairly similar, though there are some differences between 9 m and 16 m and below 33 m. The mean VGP interpretation is significantly different from the others.

magnetite in eight of these samples, but that signal could not be clearly separated out from the other components in MAX UnMix. Pyrrhotite is difficult to definitively identify in this suite of room-temperature rock magnetic analyses because gyroremanent and rotational remanent magnetizations were not specifically probed.

The demagnetization routine revealed three magnetic components in most MR1 samples: a viscous remanence component eliminated during the low-temperature and alternating field steps; a present local field component found with blocking temperatures between 100–280°C; and a high-temperature component with blocking temperatures between 270–675°C (**Figure 3**). Some of the high-temperature components with blocking temperatures below 400°C are suggestive of pyrrhotite (59 specimens), but those that do not fully demagnetize until higher temperatures represent magnetite (57 specimens) or hematite (22 specimens) grains that are more likely to be primary in nature. Only 40 of the high-temperature components (29%) were able to be fit as lines heading to the origin. There has been support for using plane fits in statistical analyses where line fits are not appropriate (e.g., McFadden and McElhinny, 1988), but plane fits did not appear robust for this work. When plane fits were used for the high-temperature components of samples, the best-fit results became biased towards the direction of the few existing line fits. This obscured the actual directional trends and polarity of the high-temperature components since a small number of samples were having an outsized impact on the rest. Instead, we chose to utilize anchored line fits for the high-temperature components of samples that had stable endpoints that did not approach the origin. These anchored fits are utilized in the remainder of our analyses (although samples that could be fit with a line without anchoring are outlined in red in **Figure 4** and **Supplementary Figure S3**). Only twelve samples were not able to be fit with anchored lines, and five samples were not included in directional analysis because of their unusual low-temperature fits.

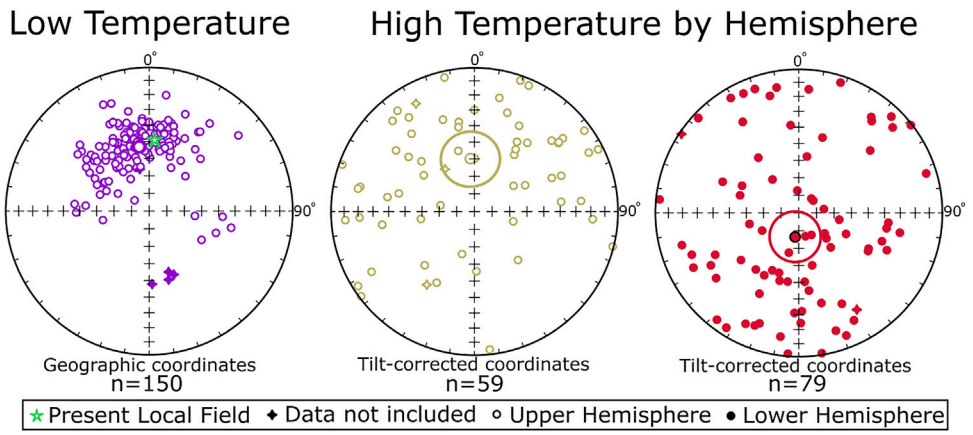

FIGURE 5 | Paleomagnetic Directions for MR1 samples. Equal area plots for low-temperature components and high-temperature components, separated into upper and lower hemispheres. The present local field when the core was collected in July 2010 (D = 2.916°, I = −49.602°) is indicated with a green star on the low temperature panel. The low-temperature fits cluster close to the present local field (Fisher mean D = 350.3°, I = −45.6°, α95 = 3.4°, n = 150. Geographic coordinates). The high-temperature fits have more spread (Upper Hemisphere Fisher mean D = 355.5°, I = −59.7°, α95 = 16.2, n = 59. Lower Hemisphere Fisher mean D = 188.9°, I = 76.3°, α95 = 14.4°, n = 79. Tilt-corrected coordinates). Values for n represent fits not hidden, so they do not include the five samples with anomalous low-temperature components.

The low-temperature directions cluster well (D = 350.3°, I = −45.6°, α95 = 3.4°, n = 150) near the present local field (for July 2010 D = 2.916°, I = −49.602°) and are thus interpreted as a modern overprint (**Figure 5**). Five samples were not included in the later analyses because their low-temperature directions were in the opposite hemisphere from all the other samples. The high-temperature components do not show as clear a trend, though clusters can be identified in the upper and lower hemispheres (**Figure 5**). A paleomagnetic conglomerate test was applied to all the tilt-corrected high-temperature directions using the Bayesian approach described by Heslop and Roberts (2018). When the high-temperature lower-hemisphere components were flipped (adding 180° to the declination and reversing the sign of the inclination), the Bayes Factor and $p(H_A|R)$ value were both 2.58×10^{-28}. With these values, there is very strong support for a unimodal distribution (Heslop and Roberts, 2018), which is expected from flipping reversed samples into the same hemisphere as normal samples. As such, we can expect the unaltered data to show a non-unimodal distribution. Overall, this supports the use of our interpreted directions for magnetostratigraphy, though the use of anchored fits instead of line fits suggests a level of caution is necessary.

Multiple magnetic reversals were identified in MR1 by plotting the samples stratigraphically to determine polarity chrons. The virtual geomagnetic poles (VGPs) of the high-temperature component directions of MR1 were plotted as an angle from the mean VGP of that dataset, calculated after flipping all the lower hemisphere directions to the upper hemisphere. Samples with a mean angular deviation (MAD) ≤ 10° were treated with higher confidence. Where the characteristic remanent direction of two or more samples crossed the 0° line from the VGP, it was treated as a magnetic reversal and used in assigning magnetic chrons for MR1 (**Figure 4**). In the same manner, the angle between the VGP of the high-temperature component directions and the pole calculated for the Canning Basin in Hansma et al. (2015) and for Gondwana at 370 Ma in Torsvik et al. (2012) was calculated and plotted to assign chrons as a comparison to this dataset (**Supplementary Figure S3**). A comparison of the three magnetostratigraphic records is shown in **Figure 4**. The assigned chrons are largely similar for the Torsvik and Hansma poles, but the magnetostratigraphy using the mean VGP from this dataset shows significant differences from the other two. This is due to the similarity between the Torsvik and Hansma paleopoles, which underscores the importance of the paleopoles used in these magnetostratigraphic calculations.

High-reversal rates like those proposed for the late Devonian Period (Shcherbakova et al., 2019; Hawkins et al., 2021) can be difficult to test if sampling density is low. However, detailed sampling of this core, with samples spaced on average 25 cm apart (representing ~10,000–30,000 years resolution), means that the frequent reversals recorded here (**Figure 4**) are consistent with a high-reversal-rate field.

5 DISCUSSION

Concerns have been raised about prior paleomagnetic analyses of the Canning Basin and their potential to be used for magnetostratigraphy (Bilardello, 2019; van der Boon et al., 2021, in review); this study provides an internal consistency check as this same set of MR1 samples was also interpreted as part of the Playton et al. (2016) analysis of the Canning Basin. Their magnetostratigraphic interpretation can be seen compared to the three made here in **Figure 4**. The mean VGP chrons differ significantly from all the other interpretations, suggesting that this is not a reliable pole for this basin probably due to the use of anchored line-fits. There is an overall agreement between the sets

of chrons assigned in our study using the Torsvik et al. (2012), Hansma et al. (2015) poles and the independent interpretations of Playton et al. (2016). However, there are notable differences between 9 m and 16 m depth and below 33 m depth, where the Torsvik et al. (2012), Hansma et al. (2015) interpretations primarily show normal polarity while the Playton et al. (2016) interpretation is largely reversed. The discrepancies near the beginning of the records may be attributable to the high MAD, anchored fits that this analysis used to mark many of the lowest chrons. Additionally, the samples at the base of the record are spaced further apart than those near the top and several are high MAD fits. Higher parts of the record have more components with low MAD values and line fits, which give greater confidence to those interpretations than those chrons assigned below 33 m depth. Overall, the similarities between the chrons assigned here and those independently analyzed and assigned in Playton et al. (2016) indicate that this is a viable magnetostratigraphic record for the late Devonian Canning Basin and can be used for basinal correlations especially if paired with litho-, bio-, or chemo-stratigraphy. For example, this magnetostratigraphic record agrees with many of the paleomagnetic tie points of Hillbun et al. (2016), which shows those points in relation to carbon isotope chemostratigraphy, conodont biostratigraphy, and third-order sequence stratigraphy. These other records can be used for basinal correlation where the paleomagnetic tie points do not align, like the major carbon isotope excursion and maximum flooding surface present at the ambiguous 15 m depth tie point (Hillbun et al., 2016).

The rock magnetic data for MR1 also indicates that these samples should be viable recorders of the primary magnetic signals necessary for magnetostratigraphy. Rock magnetic data reveal the minerals that record the magnetic directions in a sample, which is helpful for understanding their potential as primary signatures. Based on analyses of room-temperature coercivity spectra and thermal demagnetization data, the magnetic minerals seen in MR1 were goethite, hematite, pigmentary hematite, and magnetite/pyrrhotite (**Figure 2**). A high-coercivity and high-temperature hematite component was interpreted to be detrital, following Swanson-Hysell et al. (2019); eleven samples analyzed for rock magnetism contained this in addition to magnetite and/or goethite. Notably, these samples contained low MAD (average: 12.32°, four samples ≤10°, one sample without an anchored fit), which gives them greater confidence. A lower-coercivity and lower-temperature pigmentary hematite component was found in eight samples analyzed, all of which also contained magnetite. These had slightly lower MADs (average: 11.95°, three samples ≤10°, two samples without an anchored fit) but had fewer samples below the high-confidence MAD threshold. The eight samples had depths between 28.56 and 38.99 m, placing them in the area of the magnetostratigraphic record with lower overall confidence and the most significant differences between the assigned chrons and the Playton et al. (2016) analysis (**Figure 4**). Only one sample did not contain the low-coercivity magnetite or pyrrhotite component. Overall, these twenty samples with the low-coercivity component had an average MAD of 12.16° (seven samples ≤10°, four samples without an anchored fit). In general, the best high-temperature fits for MR1 were in the samples that contained hematite, since more of those samples had anchored fits with MADs ≤10° compared to those containing pigmentary hematite. The lowest confidence fits were in the lower parts of the core that contained pigmentary hematite, where fewer samples had anchored fits and MADs ≤10°.

The samples containing hematite give greater confidence in the primary nature of the magnetic signal recorded. This hematite is inferred to be detrital; therefore it could be accompanied by inclination shallowing, which would be vital to determine and potentially correct for before utilizing the paleomagnetic pole direction (Tauxe et al., 2008). The detrital phases, like the coarser-grained detrital hematite and magnetite, also demagnetize at higher temperatures than the diagenetic pigmentary hematite and pyrrhotite. Higher blocking temperatures make those minerals more likely to preserve the primary magnetic signature of the rocks and are thus treated with higher confidence. It is also notable that, unlike MR1, the WK1 samples lack rock magnetic data. Additionally they had low blocking temperatures with 67 out of 73 samples losing more than 90% of their initial magnetization by 320°C. These two factors led to concerns about the primary nature of the magnetization in WK1, so those samples were not included in the magnetostratigraphic comparisons made here (see **Supplementary Figures S5, S6** for equal area plots, Fisher means, and magnetostratigraphic columns).

Combining these rock magnetic and paleomagnetic interpretations, **Figures 6** and **Supplementary Figure S4** shows the results of separating the MR1 samples based on the blocking temperatures of their high-temperature components to roughly attempt to link magnetic mineralogy to directional components. Samples that demagnetized below 350°C, consistent with pyrrhotite, are mainly located below 33 m depth, where there are larger differences between this interpretation and those from Playton et al. (2016). This is consistent with the rock magnetic data that shows diagenetic minerals in those lower samples, which also have overall high MADs. This lower temperature pole overlaps with that from samples with blocking temperatures between 350°C and 600°C that are interpreted as being carried by magnetite. These minerals could be primary magnetic recorders as the pole directions does not plot near the present local field or the Kiaman-aged overprint [a Carboniferous strong reversed superchron during which many Devonian rocks were remagnetized including in Gondwana, van der Boon et al. (2021, in review); Schmidt et al. (1986)] (**Figure 6**). Samples with blocking temperatures above 600°C were interpreted to contain hematite, potentially detrital hematite or a mixture of pigmentary and detrital hematite. These hematite samples correspond to areas of the magnetostratigraphic record that are consistent with the Playton et al. (2016) interpretation and line up well with the mean pole for this dataset (**Figure 6**). Although the error is large, these samples have a pole direction that is located near the Kiaman overprint pole and/or between the present local field and the Kiaman-aged

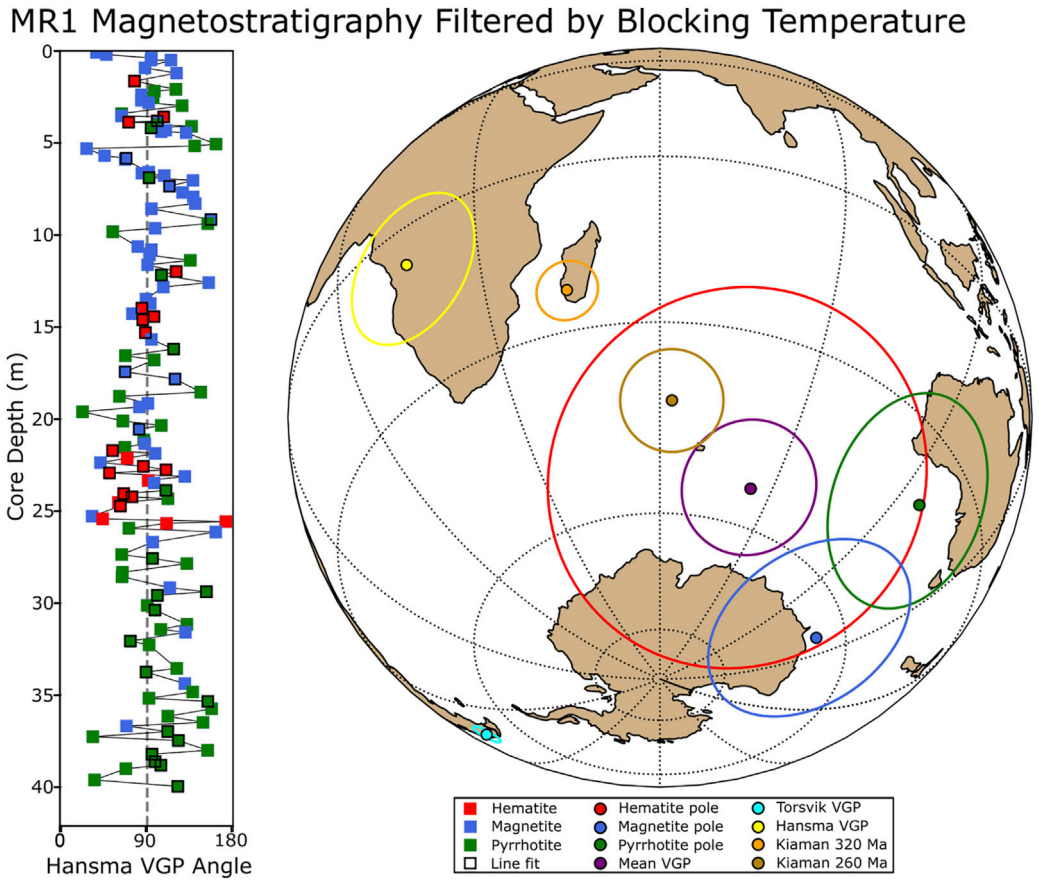

FIGURE 6 | MR1 directional data with mineralogy and MR1 pole positions. The MR1 VGPs plotted as an angle from the paleopole calculated by Hansma et al. (2015) for the Canning Basin and then color coded by mineralogy interpreted from blocking temperatures. Hematite (red) above 600°C, magnetite (blue) between 350°C and 600°C, pyrrhotite (green) below 350°C. Pole positions with A95 shown in spherical projection [red: hematite specimens only, blue: magnetite specimens only, green: pyrrhotite specimens only, purple: mean VGP, yellow: Torsvik et al. (2012) pole for Gondwana at 370 Ma, cyan: Hansma et al. (2015) pole for Canning Basin, orange: Gondwana Kiaman overprint from Torsvik et al. (2012) at 320 Ma, brown: Gondwana Kiaman overprint from Torsvik et al. (2012) at 260 Ma]. See **Supplementary Figure S4** for Equal Area plots and Fisher means. The hematite pole plots near the Kiaman overprint and/or between the present local field and the Kiaman overprint and is treated with the highest confidence. The pyrrhotite and magnetite poles plot do not plot near the present local field or the Kiaman overprint but do overlap with each other.

poles (**Figure 6**). However, the samples were not of reversed polarity as would be expected in a Kiaman overprint so perhaps the signal is a primary direction or samples are recording a complex signature from these two later overprints. Therefore, although this rock-magnetic data intriguingly points to variable reliability within magnetostratigraphy, more analyses of this type are needed to understand the primary or secondary nature of the paleomagnetic poles.

Despite internally consistent and viable magnetostratigraphy in the Canning Basin, correlating these records more broadly poses serious problems. There is a noted lack of good paleopoles and paleomagnetic data in general across the Devonian Period (Torsvik et al., 2012; van der Boon et al., 2021, in review). Even though many samples, like those presented here, have rock magnetic compositions that make them well qualified to preserve a primary magnetic signal, their paleomagnetic directions are often ambiguous and contradictory (e.g., Torsvik et al., 2012; van der Boon et al., 2021, in review; Hansma et al., 2015). The Devonian Period has therefore been suggested to be a hyperreversal time period and/or have a low intensity, non-dipolar field (Shcherbakova et al., 2017; Hawkins et al., 2021; Shcherbakova et al., 2019).

Combined with the lack of robust poles resulting from remagnetizations due to orogenic events and conflicting interpretations of pole paths (Wang and Van Der Voo, 1993; Suk et al., 1993), the dearth of Devonian paleomagnetic data means that the VGP angles used in **Figure 4** are not well defined, which plays a role in the differences between the assigned chrons in this study. It also suggests caution in correlating the sections studied here and in Hansma et al. (2015) more broadly than this small basin or utilizing them as the Global Polarity Timescale (e.g., Ogg, 2020). If the field was non-dipolar, the reversals may be captured and easily categorized for interbasinal

correlation, but they may not be globally correlatable. With a general lack of data and the ambiguous results for the available data, there is a persistent problem with larger scale correlations and interpretations of paleomagnetic data in the Devonian Period. The Paleozoic magnetostratigraphic time scale is poorly constrained (Becker et al., 2020) —high-resolution, carefully demagnetized analyses from a single stratigraphic section or even a single basin are not able to resolve this magnetostratigraphy suggesting a global collaborative approach with publicly shared measurement-level data is needed moving forward.

6 CONCLUSION

Rock magnetic data and magnetostratigraphy for a late Devonian core from the Lennard Shelf in the Canning Basin, western Australia are analyzed and correlate well with the independent interpretations by Playton et al. (2016). The samples contain magnetic minerals that are viable recorders of primary magnetic signatures, but the paleomagnetic data are noisy with high MADs and polarity assignments are often ambiguous. Multiple reversals are recorded in this interval and magnetostratigraphic records are created based on three different paleopoles [this dataset, the paleopole from Hansma et al. (2015), and the paleopole from Torsvik et al. (2012)]. The Hansma et al. (2015) and Torsvik et al. (2012) interpretations are largely consistent with each other and with the earlier magnetostratigraphy published by Playton et al. (2016). Despite this internal consistency and the viable primary magnetic recorders, numerous reversals and lack of a robust paleopole suggest correlation with sections beyond this geographic region could be difficult. As discussed by van der Boon et al. (2021, in review), there is much need for expanded publication of paleomagnetic data in the Devonian time-period in order to better understand ambiguous data and any connections to the weak Devonian field as well as increase the potential for global correlations. Robust and globally correlatable magnetostratigraphic records would help to refine the Devonian Global Polarity Time Scale and could be integrated with bio- and chemo-stratigraphy to shed light on the timing, rates, and potential causes of the Frasnian-Famennian mass extinction.

DATA AVAILABILITY STATEMENT

The datasets presented in this study can be found in online repositories. The names of the repository/repositories and accession number(s) can be found below: https://earthref.org/MagIC/19274/e5ab18fe-735d-4025-97b8-78d48a951fa8, https://earthref.org/MagIC/19273/ac274eec-b4f3-4e22-91a3-131f8839d547, https://earthref.org/MagIC/19349, https://earthref.org/MagIC/19348.

AUTHOR CONTRIBUTIONS

PM, TP, ET, RH, PH, and JK initiated and executed the Canning Basin Chronostratigraphy Project and field campaign. JK brought forward Winkie drill methodology to the project. TR and JK formulated the sampling technique and project goals. SS and PJ performed laboratory analyses. TG and SS analyzed the data. TG and SS drafted figures and wrote the manuscript with contributions from TP, PJ, and RH.

FUNDING

Funding was supplied by the Australian Research Council Linkage Program (grant LP0883812), ARC-QEII Grant Program, ARC-DORA-3 Grant Program, MERIWA, WAERA, CSIRO, Buru, Chevron Australian Business Unit, Chevron Energy Technology Company, the University of Greenwich, and Chemostrat, Ltd. PJ is supported by CAPES and FAPESP grant #2016/24870-2 and #2019/06709-8. While collecting laboratory analyses, SPS was supported by a NSF Graduate Research Fellowship. TG was supported by a Dartmouth College Senior Fellowship.

ACKNOWLEDGMENTS

We especially thank the Aboriginal tribes of the Gooniyandi (Kuniandi) people, who allowed us to conduct this research on their sacred lands. We would like to acknowledge Matthew Diamond and Steven Skinner for aid in sample preparation; Isaac Hilburn for lab discussions and data archiving; and Kelly Hillbun for co-leading field observations and sample collection. Field support and safety assistance were provided by Wundargoodie Aboriginal Safaris (Colin and Maria Morgan and family and crew), the Geological Survey of Western Australia, and the Chevron Australian Business Unit. Thanks to the Mimbi Community and Mount Pierre Station for field area access and resources. Thanks to R. Addenbrooke, A. Duffy, G. Beacher, T. Holland, S. Shoepfer, U. Singh, M. Thorp, and P. Ward for field assistance. PH and RH publish with the permission of the Executive Director of the Geological Survey of Western Australia.

SUPPLEMENTARY MATERIAL

The Supplementary Material for this article can be found online at: https://www.frontiersin.org/articles/10.3389/feart.2021.757749/full#supplementary-material

REFERENCES

Bambach, R. K., Knoll, A. H., and Sepkoski, J. J. (2002). Anatomical and Ecological Constraints on Phanerozoic Animal Diversity in the marine Realm. *Proc. Natl. Acad. Sci.* 99, 6854–6859. doi:10.1073/pnas.092150999

Becker, R. T., Marshall, J. E. A., Da Silva, A.-C., Agterberg, F. P., Gradstein, F. M., and Ogg, J. G. (2020). "The Devonian Period," in *Geologic Time Scale 2020*. 1 edn (Amsterdam, Netherlands: Elsevier), 2, 733–810. doi:10.1016/b978-0-12-824360-2.00022-x

Bilardello, D. (2019). Civilized Magnetist's Deadly Sins. *IRM Q.* 28, 12–20.

Butler, R. F. (1992). "Geochronological Applications," in *Paleomagnetism: Magnetic Domains to Geologic Terrances*. 1 edn. Boston, MA: Blackwell Scientific Publications, 159–182.

Ernst, R. E., and Youbi, N. (2017). How Large Igneous Provinces Affect Global Climate, Sometimes Cause Mass Extinctions, and Represent Natural Markers in the Geological Record. *Palaeogeogr. Palaeoclimatol. Palaeoecol.* 478, 30–52. doi:10.1016/j.palaeo.2017.03.014

Hansma, J., Tohver, E., Yan, M., Trinajstic, K., Roelofs, B., Peek, S., et al. (2015). Late Devonian Carbonate Magnetostratigraphy from the Oscar and Horse Spring Ranges, Lennard Shelf, Canning Basin, Western Australia. *Earth Planet. Sci. Lett.* 409, 232–242. doi:10.1016/j.epsl.2014.10.054

Hawkins, L. M. A., Anwar, T., Shcherbakova, V. V., Biggin, A. J., Kravchinsky, V. A., Shatsillo, A. V., et al. (2019). An Exceptionally Weak Devonian Geomagnetic Field Recorded by the Viluy Traps, Siberia. *Earth Planet. Sci. Lett.* 506, 134–145. doi:10.1016/j.epsl.2018.10.035

Hawkins, L., Grappone, J., Sprain, C., Saengduean, P., Sage, E., Sheikerra, T.-C., et al. (2021). Intensity of the Earth's Magnetic Field: Evidence for a Mid-paleozoic Dipole Low. *Proc. Natl. Acad. Sci.* 118, 1–8. doi:10.1073/pnas.2017342118

Heslop, D., and Roberts, A. P. (2018). A Bayesian Approach to the Paleomagnetic Conglomerate Test. *J. Geophys. Res. Solid Earth* 123, 1132–1142. doi:10.1002/2017jb014526

Hillbun, K., Playton, T. E., Tohver, E., Ratcliffe, K., Trinajstic, K., Roelofs, B., et al. (2015). Upper Kellwasser Carbon Isotope Excursion Pre-dates the F-F Boundary in the Upper Devonian Lennard Shelf Carbonate System, Canning Basin, Western Australia. *Palaeogeogr. Palaeoclimatol. Palaeoecol.* 438, 180–190. doi:10.1016/j.palaeo.2015.07.035

Hillbun, K., Playton, T. E., Katz, D. A., Tohver, E., Trinajstic, K., Haines, P. W., et al. (2016). "Correlation and Sequence Stratigraphic Interpretation of Upper Devonian Carbonate Slope Facies Using Carbon Isotope Chemostratigraphy, Lennard Shelf, Canning Basin, Western Australia," in *New Advances in Devonian Carbonates: Outcrop Analogs, Reservoirs and Chronostratigraphy*. Editors T. Playton, C. Kerans, and J. Weissenberger (Tulsa, OK: SEPM, Special Publication 107), 302–318. doi:10.2110/sepmsp.107.09

Hounslow, M. W., Domeier, M., and Biggin, A. J. (2018). Subduction Flux Modulates the Geomagnetic Polarity Reversal Rate. *Tectonophysics* 742-743, 34–49. doi:10.1016/j.tecto.2018.05.018

Kiessling, W., Flügel, E., and Golonka, J. (2003). Patterns of Phanerozoic Carbonate Platform Sedimentation. *Lethaia* 36, 195–225. doi:10.1080/00241160310004648

Kirschvink, J. L., Kopp, R. E., Raub, T. D., Baumgartner, C. T., and Holt, J. W. (2008). Rapid, Precise, and High-Sensitivity Acquisition of Paleomagnetic and Rock-Magnetic Data: Development of a Low-Noise Automatic Sample Changing System for Superconducting Rock Magnetometers. *Geochem. Geophys. Geosyst.* 9, 1–18. doi:10.1029/2007gc001856

Kirschvink, J. L. (1980). The Least-Squares Line and Plane and the Analysis of Palaeomagnetic Data. *Geophys. J. Int.* 62, 699–718. doi:10.1111/j.1365-246x.1980.tb02601.x

Langereis, C. G., Krijgsman, W., Muttoni, G., and Menning, M. (2010). Magnetostratigraphy Concepts, Definitions, and Applications. *nos* 43, 207–233. doi:10.1127/0078-0421/2010/0043-0207

Lu, M., Lu, Y., Ikejiri, T., Sun, D., Carroll, R., Blair, E. H., et al. (2021). Periodic Oceanic Euxinia and Terrestrial Fluxes Linked to Astronomical Forcing during the Late Devonian Frasnian-Famennian Mass Extinction. *Earth Planet. Sci. Lett.* 562, 116839. doi:10.1016/j.epsl.2021.116839

Ma, X., Gong, Y., Chen, D., Racki, G., Chen, X., and Liao, W. (2016). The Late Devonian Frasnian-Famennian Event in South China - Patterns and Causes of Extinctions, Sea Level Changes, and Isotope Variations. *Palaeogeogr. Palaeoclimatol. Palaeoecol.* 448, 224–244. doi:10.1016/j.palaeo.2015.10.047

Maxbauer, D. P., Feinberg, J. M., and Fox, D. L. (2016). MAX UnMix: A Web Application for Unmixing Magnetic Coercivity Distributions. *Comput. Geosci.* 95, 140–145. doi:10.1016/j.cageo.2016.07.009

McFadden, P. L., and McElhinny, M. W. (1988). The Combined Analysis of Remagnetization Circles and Direct Observations in Palaeomagnetism. *Earth Planet. Sci. Lett.* 87, 161–172. doi:10.1016/0012-821x(88)90072-6

Ogg, J. G. (2020). "Geomagnetic Polarity Time Scale," in *Geologic Time Scale 2020*. 1 edn (Amsterdam, Netherlands: Elsevier), 1, 159–192. doi:10.1016/b978-0-12-824360-2.00005-x

Percival, L. M. E., Davies, J. H. F. L., Schaltegger, U., De Vleeschouwer, D., Da Silva, A.-C., and Föllmi, K. B. (2018). Precisely Dating the Frasnian-Famennian Boundary: Implications for the Cause of the Late Devonian Mass Extinction. *Sci. Rep.* 8, 9578. doi:10.1038/s41598-018-27847-7

Perrin, M., and Shcherbakov, V. (1997). Paleointensity of the Earth's Magnetic Field for the Past 400 Ma: Evidence for a Dipole Structure during the Mesozoic Low. *J. Geomagn. Geoelec.* 49, 601–614. doi:10.5636/jgg.49.601

Peters, C., and Dekkers, M. J. (2003). Selected Room Temperature Magnetic Parameters as a Function of Mineralogy, Concentration and Grain Size. *Phys. Chem. Earth, Parts A/B/C* 28, 659–667. doi:10.1016/s1474-7065(03)00120-7

Playford, P., Hocking, R., Cockbain, A., Becker, R., and House, M. (2009). *Devonian Reef Complexes of the Canning Basin, Western Australia Geological Survey of Western Australia Bulletin 145 Devonian Ammonoid Biostratigraphy of the Canning Basin*. Perth, Australia: Geological Survey of Western Australia, 415–439.

Playton, T. E., Hocking, R. M., Tohver, E., Hillbun, K., Haines, P. W., Trinajstic, K., et al. (2016). "Integrated Stratigraphic Correlation of Upper Devonian Platform-To-Basin Carbonate Sequences, Lennard Shelf, Canning Basin, Western Australia: Advances in Carbonate Margin-To-Slope Sequence Stratigraphy and Stacking Patterns," in *New Advances in Devonian Carbonates: Outcrop Analogs, Reservoirs and Chronostratigraphy*. Editors T. Playton, C. Kerans, and J. Weissenberger (Tulsa, OK: SEPM, Special Publication), 107, 248–301.

Ricci, J., Quidelleur, X., Pavlov, V., Orlov, S., Shatsillo, A., and Courtillot, V. (2013). New 40Ar/39Ar and K-Ar Ages of the Viluy Traps (Eastern Siberia): Further Evidence for a Relationship with the Frasnian-Famennian Mass Extinction. *Palaeogeogr. Palaeoclimatol. Palaeoecol.* 386, 531–540. doi:10.1016/j.palaeo.2013.06.020

Sallan, L. C., and Coates, M. I. (2010). End-Devonian Extinction and a Bottleneck in the Early Evolution of Modern Jawed Vertebrates. *Proc. Natl. Acad. Sci.* 107, 10131–10135. doi:10.1073/pnas.0914000107

Schmidt, P. W., Embleton, B. J. J., Cudahy, T. J., and Powell, C. M. (1986). Prefolding and Premegakinking Magnetizations from the Devonian Comerong Volcanics, New south wales, australia, and Their Bearing on the Gondwana Pole Path. *Tectonics* 5, 135–150. doi:10.1029/tc005i001p00135

Sepkoski, J. J. (2002). A Compendium of Fossil marine Animal Genera. *Bulletins Am. Paleontol.* 363, 1–560.

Shcherbakova, V. V., Biggin, A. J., Veselovskiy, R. V., Shatsillo, A. V., Hawkins, L. M. A., Shcherbakov, V. P., et al. (2017). Was the Devonian Geomagnetic Field Dipolar or Multipolar? Palaeointensity Studies of Devonian Igneous Rocks from the Minusa Basin (Siberia) and the Kola Peninsula Dykes, Russia. *Geophys. J. Int.* 209, 1265–1286. doi:10.1093/gji/ggx085

Shcherbakova, V. V., Bakhmutov, V. G., Thallner, D., Shcherbakov, V. P., Zhidkov, G. V., and Biggin, A. J. (2019). Ultra-low Palaeointensities from East European Craton, Ukraine Support a Globally Anomalous Palaeomagnetic Field in the Ediacaran. *Geophys. J. Int.* 220, 1928–1946. doi:10.1093/gji/ggz566

Suk, D., Van Der Voo, R., and Peacor, D. R. (1993). Origin of Magnetite Responsible for Remagnetization of Early Paleozoic Limestones of new york State. *J. Geophys. Res.* 98, 419–434. doi:10.1029/92jb01323

Swanson-Hysell, N. L., Fairchild, L. M., and Slotznick, S. P. (2019). Primary and Secondary Red Bed Magnetization Constrained by Fluvial Intraclasts. *J. Geophys. Res. Solid Earth* 124, 4276–4289. doi:10.1029/2018JB017067

Tauxe, L., Kodama, K. P., and Kent, D. V. (2008). Testing Corrections for Paleomagnetic Inclination Error in Sedimentary Rocks: A Comparative Approach. *Phys. Earth Planet. Inter.* 169, 152–165. doi:10.1016/j.pepi.2008.05.006

Tauxe, L., Shaar, R., Jonestrask, L., Swanson-Hysell, N. L., Minnett, R., Koppers, A. A. P., et al. (2016). Pmagpy: Software Package for Paleomagnetic Data Analysis and a Bridge to the Magnetics Information Consortium (Magic) Database. *Geochem. Geophys. Geosyst.* 17, 2450–2463. doi:10.1002/2016gc006307

Torsvik, T. H., Van der Voo, R., Preeden, U., Mac Niocaill, C., Steinberger, B., Doubrovine, P. V., et al. (2012). Phanerozoic Polar Wander, Palaeogeography and Dynamics. *Earth-Science Rev.* 114, 325–368. doi:10.1016/j.earscirev.2012.06.007

Tyler, I. M., Hocking, R. M., and Haines, P. W. (2012). Geological Evolution of the Kimberley Region of Western Australia. *Episodes* 35, 298–306. doi:10.18814/epiiugs/2012/v35i1/029

van der Boon, A., Biggin, A., Thallner, D., Hounslow, M., Bono, R., Nawrocki, J., et al. (2021). A Persistent Non-uniformitarian Paleomagnetic Field in the Devonian? *Earth Sci. Rev.* doi:10.31223/X53W56 in review.

Wang, Z., and Van Der Voo, R. (1993). Pervasive Remagnetization of Paleozoic Rocks Acquired at the Time of Mesozoic Folding in the south china Block. *J. Geophys. Res.* 98, 1729–1741. doi:10.1029/92jb02405

Conflict of Interest: Authors PM and TP were employed by the company the Chevron Energy Technology Company. Funding for the fieldwork and laboratory analyses was provided by the Chevron Australian Business Unit, Chevron Energy Technology Company and Chemostrat, LTD.

The remaining authors declare that the research was conducted in the absence of any commercial or financial relationships that could be construed as a potential conflict of interest.

Publisher's Note: All claims expressed in this article are solely those of the authors and do not necessarily represent those of their affiliated organizations, or those of the publisher, the editors and the reviewers. Any product that may be evaluated in this article, or claim that may be made by its manufacturer, is not guaranteed or endorsed by the publisher.

Copyright © 2021 Green, Slotznick, Jaqueto, Raub, Tohver, Playton, Haines, Kirschvink, Hocking and Montgomery. This is an open-access article distributed under the terms of the Creative Commons Attribution License (CC BY). The use, distribution or reproduction in other forums is permitted, provided the original author(s) and the copyright owner(s) are credited and that the original publication in this journal is cited, in accordance with accepted academic practice. No use, distribution or reproduction is permitted which does not comply with these terms.